TGF-β triggers rapid fibrillogenesis via a novel TβRII-dependent fibronectin-trafficking mechanism

Archana Varadaraj[a], Laura M. Jenkins[a,†], Priyanka Singh[a,†], Anindya Chanda[b], John Snider[a], N.Y. Lee[c], Ayelet R. Amsalem-Zafran[d], Marcelo Ehrlich[e], Yoav I. Henis[d], and Karthikeyan Mythreye[a,f,*]

[a]Department of Chemistry and Biochemistry and [f]Department of Drug Discovery and Biomedical Sciences, University of South Carolina, Columbia, SC 29208; [b]Department of Environmental Health Sciences, University of South Carolina, Columbia, SC 29201; [c]Division of Pharmacology, College of Pharmacy, Ohio State University, Columbus, OH 43210; [d]Department of Neurobiology and [e]Department of Cell Research and Immunology, Faculty of Life Sciences, Tel Aviv University, Tel Aviv 69978, Israel

ABSTRACT **Fibronectin (FN) is a critical regulator of extracellular matrix (ECM) remodeling through its availability and stepwise polymerization for fibrillogenesis. Availability of FN is regulated by its synthesis and turnover, and fibrillogenesis is a multistep, integrin-dependent process essential for cell migration, proliferation, and tissue function. Transforming growth factor β (TGF-β) is an established regulator of ECM remodeling via transcriptional control of ECM proteins. Here we show that TGF-β, through increased FN trafficking in a transcription- and SMAD-independent manner, is a direct and rapid inducer of the fibrillogenesis required for TGF-β–induced cell migration. Whereas TGF-β signaling is dispensable for rapid fibrillogenesis, stable interactions between the cytoplasmic domain of the type II TGF-β receptor (TβRII) and the FN receptor (α5β1 integrin) are required. We find that, in response to TGF-β, cell surface–internalized FN is not degraded by the lysosome but instead undergoes recycling and incorporation into fibrils, a process dependent on TβRII. These findings are the first to show direct use of trafficked and recycled FN for fibrillogenesis, with a striking role for TGF-β in this process. Given the significant physiological consequences associated with FN availability and polymerization, our findings provide new insights into the regulation of fibrillogenesis for cellular homeostasis.**

Monitoring Editor
Kunxin Luo
University of California, Berkeley

Received: Aug 17, 2016
Revised: Feb 22, 2017
Accepted: Feb 27, 2017

INTRODUCTION

The extracellular matrix (ECM) is a key player in regulating cell differentiation, growth, and motility during wound-healing and fibrotic responses. Growth factors, particularly transforming growth factor β (TGF-β), can regulate the ECM by increasing fibronectin (FN) synthesis (Ignotz and Massague, 1986; Allen-Hoffmann *et al.*, 1988; Roberts *et al.*, 1988; Bortell *et al.*, 1994; Hocevar and Howe, 2000; Biname *et al.*, 2008). The bulk of TGF-β transcriptional responses, including FN transcription, are mediated through phosphorylation-dependent activation of the type I receptor (TβRI/ALK5) and SMAD2/3 or SMAD1/5 (Ignotz and Massague, 1986; de Caestecker, 2004; Daly *et al.*, 2008), which requires the constitutive kinase activity of the type II receptor (TβRII; Massague *et al.*, 1991).

FN produced by the cell can be assembled in a stepwise manner by most cell types to produce matrix-associated FN in a process termed fibrillogenesis (Mao and Schwarzbauer, 2005). In addition to providing a structural scaffold, fibrillogenesis is key to physiological cell repair, motility, and adhesion, thus making it a highly regulated

This article was published online ahead of print in MBoC in Press (http://www.molbiolcell.org/cgi/doi/10.1091/mbc.E16-08-0601) on March 15, 2017.

†These authors contributed equally to this work.

The authors declare no competing financial interests.

*Address correspondence to: Karthikeyan Mythreye (mythreye@sc.edu).

Abbreviations used: CHX, cyclohexamide; DOC, deoxycholate; ECM, extracellular matrix; FN, fibronectin; FRAP, fluorescence recovery after photobleaching; GFP, green fluorescent protein; HFF, human foreskin fibroblast; RFP, red fluorescent protein; Rh, rhodamine; TβRII, Type II TGF-β receptor; TGF-β, transforming growth factor β; TIRF, total internal reflection fluorescence.

process affected by the availability of FN, activation state of the FN receptor, and rate of remodeling (Schwarzbauer and Sechler, 1999; Schwarzbauer and DeSimone, 2011). Availability and balance of soluble and matrix-incorporated FN are also critical because soluble or dimeric FN can drive the epithelial-to-mesenchymal transition, whereas matrix-associated polymeric FN can decrease cancer cell invasiveness (Ruoslahti, 1984; Saulnier *et al.*, 1996; Shi *et al.*, 2014). Such opposing functions point to the significance of soluble versus matrix FN regulation.

Several studies have examined the molecular requirements and dynamic nature of fibrillogenesis and its biomechanical properties (Erickson *et al.*, 1981; Erickson and Carrell, 1983; Lotz *et al.*, 1989; Danen *et al.*, 2002; Mao and Schwarzbauer, 2005). Initiation and completion of fibrillogenesis are not always very efficient processes because a significant portion of FN that is engaged with its receptor might not be used/incorporated into fibrils (Pankov *et al.*, 2000). However, once incorporated, remodeling of matrix-incorporated FN can also occur at the level of protein turnover via either endocytosis-dependent lysosomal degradation of FN (Sottile and Chandler, 2005) or during changes in spatiotemporal control of fibrillogenesis. Such remodeling events determine cellular responses, as seen in epithelial branching morphogenesis, in which both synthesis and transient assembly of FN are observed at cleft-forming sites (Sakai *et al.*, 2003).

Integrins play key roles in fibrillogenesis: α5β1, α8β1, αvβ1, αvβ3, αIIbβ3, αvβ5, αvβ6, and αvβ8 all recognize the common integrin-binding motif Arg-Gly-Asp (RGD), which is found in many ECM components, including FN (Danen and Sonnenberg, 2003). α5β1, however, is most efficient in mediating FN matrix assembly, with compensation from other integrins also possible in the absence of α5β1 (Wu *et al.*, 1996; Yang and Hynes, 1996). We and others have also reported several interactions between the TGF-β and integrin pathways that occur through SMAD-independent mechanisms and can affect integrin signaling (Hocevar *et al.*, 1999; Bhowmick *et al.*, 2001; Galliher and Schiemann, 2006, 2007; Galliher-Beckley and Schiemann, 2008; Garamszegi *et al.*, 2010; Huck *et al.*, 2010; Mythreye *et al.*, 2013).

Whereas prior studies examined mechanisms of FN turnover and suggested specific trafficking regulation of ECM components as a mechanism for increased matrix assembly (Abraham *et al.*, 2004; Sottile and Chandler, 2005; Unlu *et al.*, 2014), whether non–matrix-incorporated, soluble ECM components are capable of returning to the cell surface has yet to be determined. Here we show that a rapid fibrillogenesis response to TGF-β in both nonmotile and motile cells precedes transcriptionally induced fibrillogenesis. We find that one mechanism for this nontranscriptional fibrillogenesis is via increased FN uptake and recycling of soluble FN. Our results reveal that internalized FN can recycle through a Rab11-dependent mechanism for fibrillogenesis, particularly in response to TGF-β stimulation. Of note, recycled and trafficked FN can constitute a significant portion of matrix-incorporated FN. We also find that TGF-β–induced rapid fibrillogenesis is largely independent of SMAD activation but requires TβRII to mediate FN recycling. Specifically, we show that this process occurs through a TβRII-α5β1–dependent interaction that is disrupted in the TβRII mutant lacking the cytoplasmic domain required for trafficking. From a broad perspective, our findings suggest that discrete sources of soluble FN could be used to build and assemble a FN matrix, which may directly affect growth factor–regulated matrix assembly and, ultimately, the rate and extent of cell differentiation, growth, and motility.

RESULTS

TGF-β1 and TGF-β2 rapidly increase fibrillogenesis

To investigate the effects of TGF-β on FN fibrillogenesis, we used two approaches: biochemical fractionation of soluble (S) FN and the fibril-associated insoluble pellet (P) FN using the detergent deoxycholate (DOC fractionation; Sechler *et al.*, 1996) and immunofluorescence microscopy to visualize FN localization and fibrillogenesis. Using these methods in human foreskin fibroblast cells (HFFs), an established cell line for FN matrix assembly (Clark *et al.*, 2005), we find that, in response to a 30-min TGF-β treatment, soluble (S) FN levels decreased, with a compensatory increase in (P) FN levels (Figure 1A). Immunolabeling of FN also revealed an increase in the appearance of FN fibrils in response to both TGF-β1 and TGF-β2 (Figure 1B), in accordance with the biochemical fractionation (Figure 1A). Consistent with the effect of TGF-β in HFF cells, a similar increase in FN- and DOC-insoluble (P) fraction of FN was observed in response to both TGF-β1 and TGF-β2 in nonfibroblast MCF10A epithelial cells (Figure 1, C and D, top, –cycloheximide [CHX]). These findings suggest a rapid response to TGF-β for fibrillogenesis in divergent cell types.

Prior studies in fibroblasts indicated that FN assembly by TGF-β can occur in the absence of protein synthesis (Allen-Hoffmann *et al.*, 1988). To examine whether TGF-β stimulated FN assembly within 30 min and was independent of protein synthesis in epithelial MCF10A cells as well, we investigated FN localization in the presence of CHX, the protein synthesis inhibitor (Figure 1D, bottom, and Supplemental Figure S1A). CHX treatment did not inhibit TGF-β–mediated increases in the appearance of FN fibrils (Figure 1D, +CHX). Consistent with no requirement for new FN synthesis, total pools of FN did not increase in cells after treatment with TGF-β for 30 min (Figure 1E). TGF-β1– and TGF-β2–induced increase in the DOC-insoluble (P) fraction of FN in MCF10A epithelial cells also remained high even in the presence of CHX (Supplemental Figure S1A). These findings indicate that TGF-β–induced fibrillogenesis in epithelial cells can be protein synthesis independent. We observed no specific accumulation of cells in any phase of the cell cycle that could have contributed to fibrillogenesis in response to 30 min of TGF-β stimulation (Supplemental Figure S1B). To confirm that the TGF-β–induced fibrils were indeed at the cell surface in MCF10A cells, we used total internal reflection fluorescence (TIRF) microscopy to image and quantify cell surface FN. In agreement with Figure 1C, we observed a significant increase in cell surface FN in response to TGF-β1 and TGF-β2 (Figure 1F). Quantitation of distinct FN structures on the cell surface was performed using a length of 3 μm as a threshold for cut-off (Coussen *et al.*, 2002; Lutz *et al.*, 2011; *Materials and Methods*). This criterion was used in all subsequent analyses of MCF10A cells. Cells with FN fluorescent puncta less than the threshold length were classified as cells lacking FN fibrils. This method of quantification was in accordance with our DOC fractionation observations (Figure 1, A and C), as TGF-β1 and TGF-β2 significantly increased the number of quantifiable FN fibrils compared with control cells (Figure 1G). To establish firmly that TGF-β was enhancing fibrillogenesis in MCF10A cells, we treated TGF-β–stimulated cells with either the functional upstream domain (FUD) peptide (a short 49-mer that binds the N-terminal sites on FN to block fibril assembly) or a matched control peptide IIIC (Tomasini-Johansson *et al.*, 2006; Shi *et al.*, 2014) as described in *Materials and Methods*. DOC fractionation of the soluble (S) FN and the fibril-associated insoluble pellet (P) FN (Figure 1H) and immunofluorescence (Figure 1I) revealed that the FUD peptide significantly abolished the observed fibril assembly mediated by TGF-β in epithelial cells compared with either TGF-β alone or TGF-β in the presence of

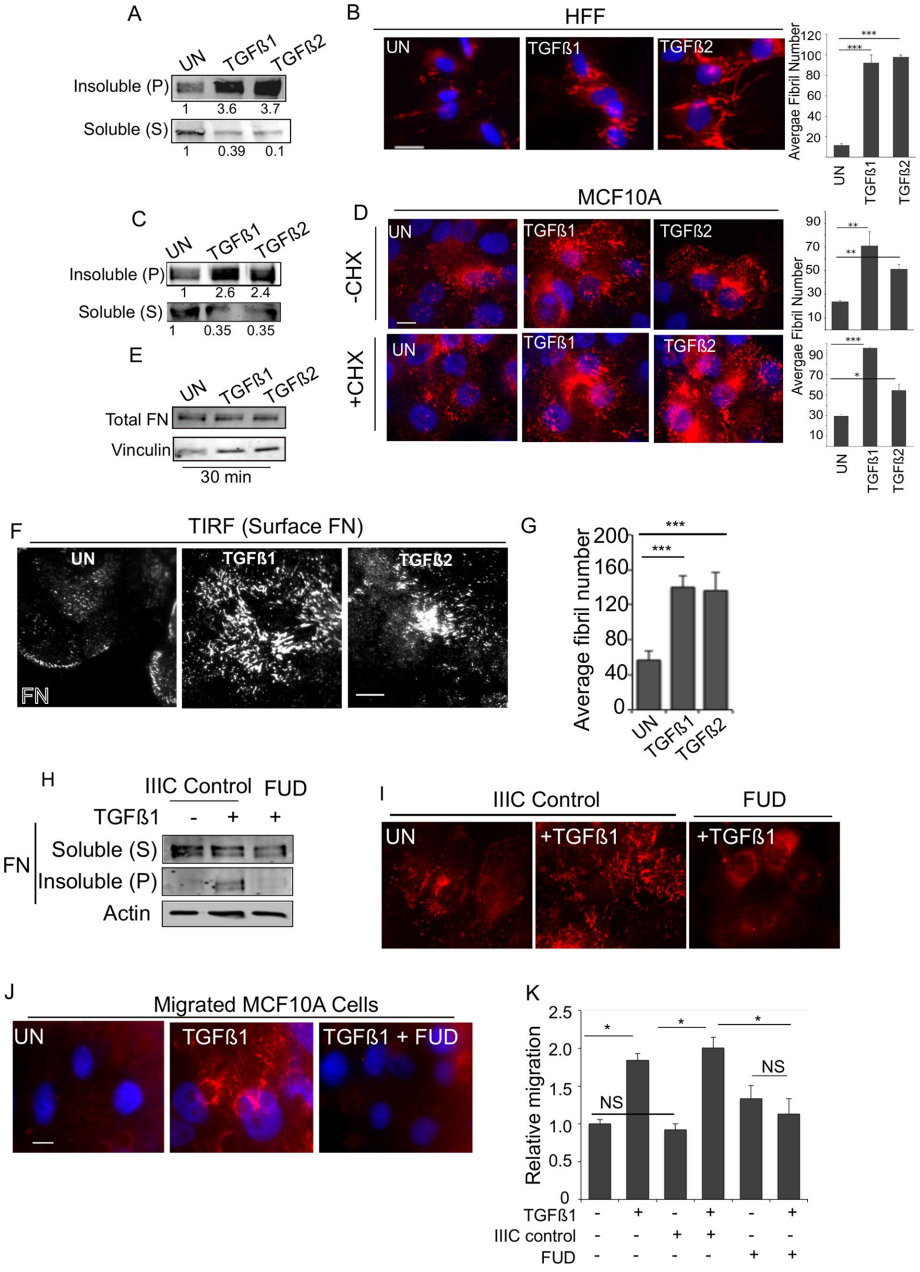

FIGURE 1: TGF-β1 and TGF-β2 rapidly increase fibrillogenesis. (A, B) HFFs were treated with TGF-β1 or TGF-β2 for 30 min and (A) DOC extraction used to fractionate DOC-soluble (S) and -insoluble (pellet (P)) pool and immunoblotted for FN, or (B) cells were immunostained using anti-FN. Right, average fibril number (*Materials and Methods*) in untreated (UN), TGF-β1–, or TGF-β2–treated cells. Fibril lengths were tracked using the NeuronJ plug-in on ImageJ. (*Materials and Methods*). (C) MCF10A cells treated with TGF-β1 or TGF-β2 for 30 min and processed for DOC extraction and immunoblotted for (S) and (P) FN as in A. (D) MCF10A cells untreated or treated with 10 ng/ml TGF-β1 or TGF-β2 for 30 min (with or without preincubation with 20 μg/ml CHX for 2 h) and immunostained for endogenous FN. Right, average fibril number in untreated (UN), TGF-β1–, or TGF-β2–treated cells. Fibril lengths were tracked using the NeuronJ plug-in on ImageJ. Scale bar, 5 μm. (E) Total MCF10A cell lysates at the indicated treatment times were lysed in SDS buffer to solubilize total FN pools ((S) and (P) combined) and immunoblotted against FN. Vinculin was used as the loading control. (F) Cells treated as in A and imaged using TIRF microscopy (penetration depth, 110 nm). Scale bar, 5 μm. (G) Average fibril number analyzed from TIRF images in untreated (UN), TGF-β1–, or TGF-β2–treated cells. Fibril lengths from F were tracked using the NeuronJ plug-in on ImageJ. (H, I) MCF10A cells were treated with 10 ng/ml TGF-β1 for 30 min (with or without 500 nM FUD peptide or the matched control IIIC peptide) and processed either (H) for DOC extraction and immunoblotting for (S) and (P) FN (actin was the loading control from the soluble pool) or (I) immunostained for FN. (J) MCF10A cells allowed to migrate for 6 h in the presence of Rh-FN as indicated in the figure. Migrated cells are captured by fixing the cells on the Transwell filter. Images of Rh-FN are representative of at least four different fields on the filter from two independent biological trials. Scale bar, 5 μm. (K) Transwell migration through FN-coated Transwells of MCF10A for 12 h either untreated or in the presence of TGF-β1 alone or with either control IIIC peptide or FUD peptide as in J and as indicated. Migrated cells were counted and plotted relative to untreated filters. Asterisks indicate significant differences as indicated (*$p < 0.05$, **$p < 0.01$, ***$p < 0.001$). Quantitation of blots is representative of a minimum of three independent trials.

a control peptide (Figure 1I and Supplemental Figure S1C)

Given that the immunofluorescence of FN and DOC fractionation were examined in nonmigrating cells and the established role of TGF-β in epithelial cell migration (Wang *et al.*, 2005; Park and Schwarzbauer, 2014), we next investigated the effect of fibrillogenesis in migrating epithelial cells. To test this, we carried out a Transwell migration assay for 6 h in the presence of exogenously added rhodamine-FN (Rh-FN; *Materials and Methods*). We found that cells that migrated in the presence of TGF-β showed distinct Rh-FN fibrils, in contrast to cells that migrated without TGF-β (Figure 1J). TGF-β–induced fibril formation in migrating cells was disrupted in the presence of FUD (Shi *et al.*, 2014), indicating that TGF-β increased FN assembly in migrating cells as well. Moreover, TGF-β–induced cell migration was disrupted by the FUD peptide (Figure 1K). The control IIIC peptide did not affect cell migration (Figure 1K) or fibrillogenesis (Supplemental Figure S1C), consistent with prior reports (Chiang *et al.*, 2009; Singh and Schwarzbauer, 2014). Together, these data suggest that TGF-β triggers rapid fibrillogenesis in migrating cells that is independent of new protein synthesis.

TGF-β type II receptor is required for fibrillogenesis

Because TGF-β1 and TGF-β2 treatments increase fibrillogenesis, we sought to determine whether this was mediated via the TGF-β receptor serine threonine kinases, which regulate both SMAD-dependent and SMAD-independent signaling (Massague, 2012). To test the contribution of the kinase activity of the type I TGF-β receptor, we used MCF10A cells and biochemically quantified the (S) and (P) FN fractions of

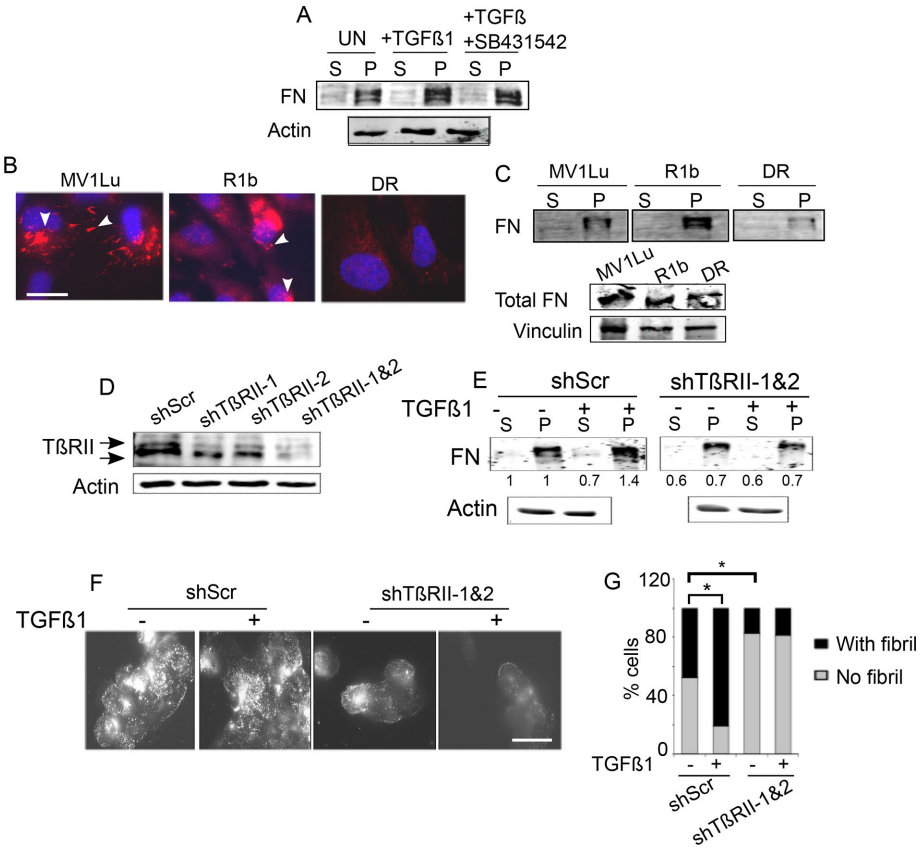

FIGURE 2: TβRII is required for fibrillogenesis. (A) MCF10A cells were preincubated with 3 μM SB431542 for 30 min before treatment with 10 ng/ml TGF-β1 for 30 min. Lysates were DOC fractionated and immunoblotted for FN. Actin was the loading control for the (S) fraction. (B, C) Either (B) Mink lung epithelial cells MV1Lu (wild type [WT] for type I, II, III TGF-β receptors), R1b (WT for type II, III), and DR (WT for type III)) were immunostained for FN or (C) cell lysates were DOC fractionated and immunoblotted for FN in the soluble (S) and insoluble (P) pools. Arrowheads indicate short fibrils and focal contacts. Scale bar, 5 μm. Immunoblot below in C shows total FN levels ((S) and (P) fractions combined) in the Mink lung cell lines. Vinculin was the loading control. (D) TβRII levels in MCF10A cells transfected with shRNAs to TβRII (shTβRII-1 and 2) or shScr to examine efficacy of knockdown. (E) Indicated MCF10A cells were treated with TGF-β1 (10 ng/ml for 30 min), DOC extracted into the (S) and (P) fractions, and immunoblotted for FN. Numbers for soluble (S) fraction are normalized to actin and pellet (P) relative to the normalized soluble pool in untreated conditions. Quantitation of blots is representative of three independent trials. (F) Cells transfected with shRNAs to TβRII (shTβRII-1 and 2) or shScr were left untreated or treated with TGF-β1 (10 ng/ml for 30 min) and immunostained for FN. Representative images. Scale bar, 3.7 μm. (G) Percentage of fibril-containing cells in the indicated conditions were quantified and plotted. Asterisks indicate significant differences (*t* test) between untreated and TGF-β1–treated samples in shScr transfectants (*$p < 0.001$) and between untreated and TGF-β1–treated samples in shTβRII (shTβRII-1 and 2) transfectants (*$p < 0.001$). Data are representative of two independent experiments.

untreated and TGF-β–treated cells in the presence of SB431542, a type I TGF-β receptor kinase (TβRI/ALK5) inhibitor that blocks SMAD2/3 and SMAD1/5 activation (Supplemental Figure S2A; Daly *et al.*, 2008). We observed an increase in the insoluble (P) fraction in the presence of SB431542 (Figure 2A), indicating that rapid fibrillogenesis is independent of TβRI kinase activity. We previously reported that regulation of fibrillogenesis by the TGF-β type III receptor (TβRIII) depends on the type II TGF-β receptor (TβRII; Mythreye *et al.*, 2013). In addition, TβRII is a well-established target of integrin signaling (Galliher and Schiemann, 2007). Hence, to test the cellular relevance of TβRI and TβRII to fibrillogenesis, we used the mink lung series of epithelial cell lines, which express either all three receptors (TβRI, TβRII, and TβRIII; Mv1Lu), only TβRII and TβRIII (R1b), or only TβRI and TβRIII (DR; Boyd and Massague, 1989; Laiho *et al.*, 1990; Wrana *et al.*, 1992), and qualitatively examined steady-state fibrillogenesis. Immunolabeling of FN (Figure 2B) revealed that Mv1Lu and R1b cells showed distinct and punctate patterns of short FN fibrils, much like untreated MCF10A cells (Figure 1D). DR cells, which lack TβRII, showed little to no FN fibrils, with only diffuse FN observed (Figure 2B) compared with Mv1Lu cells. Biochemical fractionation of the fibrils showed the least DOC-insoluble pellet fraction in the DR cells, with significantly higher amounts of pellet in the R1b cells that do not express TβRI/ALK5, despite relatively equal amounts of total FN (Figure 2C, bottom). All three cell lines expressed the primary fibronectin receptors integrin α5β1 (Supplemental Figure S2B) and were also reported to express other FN receptors (Garamszegi *et al.*, 2010). These data suggest that the differences observed could in part be due to differences in TβRII levels. To confirm this hypothesis and a role for TβRII, we transiently suppressed TβRII expression in MCF10A cells using different short hairpin RNAs (shRNAs) to TβRII (shTβRII-1, shTβRII-2, or in combination for greater knockdown; Figure 2D) and DOC-fractionated MCF10A cells to evaluate relative (S) and (P) FN fractions (Figure 2E) or examine FN by immunolabeling (Figure 2F). TGF-β1 was unable to increase the FN in the (P) pool in shTβRII cells compared with shScr cells (Figure 2E) or increase the appearance of FN fibrils (Figure 2F). Quantitation of fibrils in MCF10A shTβRII-1 and 2 cells treated with TGF-β revealed a fourfold decrease in the percentage of cells containing fibrils compared with control cells ($N = 200$; Figure 2, F and G), in concurrence with the DOC fractionation, indicating a requirement for TβRII in TGF-β–induced fibrillogenesis. shScr cells also exhibited a statistically higher number of cells containing fibrils in untreated conditions compared with shTβRII cells (***$p < 0.001$; Figure 2G). These results and the reduced baseline fibril fraction in DR cells (Figure 2, B and C) suggest that fibrillogenesis requires TβRII.

TβRII's cytoplasmic domain is required for interactions with integrin α5 and fibrillogenesis

Given the central role of integrin α5β1 in fibrillogenesis (Wennerberg *et al.*, 1996; Yang *et al.*, 1999) and the new role for TβRII in fibrillogenesis (Figure 2), we tested whether TβRII and integrin α5β1 receptors act in concert to mediate fibrillogenesis. To determine whether TβRII interacted with the subunits of the FN receptor (α5β1) at the cell surface, we carried out patch/fluorescence recovery after

photobleaching (FRAP) analyses (Henis *et al.*, 1990; Rechtman *et al.*, 2009) between integrin α5 or β1 and TβRII. This method involves patching and immobilizing one receptor by cross-linking with a double layer of immunoglobulin Gs (IgGs) and then determining the effect on the lateral diffusion of a coexpressed membrane protein, which is labeled, immobilized (in this case, by red fluorescent protein [RFP] or green fluorescent protein [GFP]), and measured by FRAP (*Materials and Methods*). Formation of mutual complexes between these proteins can reduce either the mobile fraction (R_f) or lateral diffusion coefficient (D) of the un-cross-linked protein, depending on the FRAP time scale relative to the rate of dissociation/association of the oligomer. Complex lifetimes longer than the characteristic FRAP times (stable interactions) result in reduced R_f without affecting D because bleached molecules of the un-cross-linked protein do not markedly dissociate from the immobile clusters during the FRAP measurements. On the other hand, short complex lifetimes (transient interactions) lead to several association/dissociation cycles for each fluorescence-labeled molecule during the FRAP measurement, resulting in lower D without affecting R_f. We coexpressed myc-TβRII and integrin α5-RFP (or β1-GFP) in COS7 cells and subjected the cells to patch/FRAP measurements with or without IgG cross-linking of myc-TβRII in the presence or absence of FN (Figure 3A). Integrin α5-RFP expressed alone or with myc-TβRII in the absence of IgG cross-linking exhibited similar and high lateral diffusion in the plasma membrane, with a high mobile fraction (0.91). IgG-mediated patching of myc-TβRII rendered the latter laterally immobile (Figure 3Aiv) and led to a significant reduction in R_f of integrin α5-RFP (to 0.82; Figure 3Av) without affecting the D values, which were all within the range of 0.1 ± 0.02 $\mu m^2/s$ (unpublished data). Such an effect is characteristic of stable interactions (Henis *et al.*, 1990; Rechtman *et al.*, 2009) between integrin α5 and TβRII in a fraction of the total cell surface pool. Incubation with FN somewhat further reduced the R_f values (a reduction of 0.09–0.13). However, the additional reduction was mainly due to a marginally higher R_f value before IgG cross-linking, indicating that steady-state interactions between TβRII and α5 are not largely increased by the presence of exogenous FN. Of note, an analogous reduction was observed in R_f of integrin β1-GFP upon cross-linking of coexpressed myc-TβRII (Figure 3Avi). The only difference was that, in this case, addition of FN sufficed to immobilize part of the β1-GFP cell surface population, possibly due to the multimeric nature of FN, which can cluster integrin β1 and target it to cytoskeletal structures (McKeown-Longo and Mosher, 1984; Bhatia *et al.*, 1999; Eisenberg *et al.*, 2011). These findings suggest that TβRII interacts stably at the cell surface with integrin α5β1 and this interaction persists in the presence of FN. Moreover, the interaction is exclusively with TβRII because similar studies cross-linking the type I TGF-β receptor (myc-TβRI) with integrin α5-RFP did not affect integrin α5 mobility (Figure 3Avii).

Because the cytoplasmic domain of TβRII is critical for TβRII trafficking (Murphy *et al.*, 2007) and is also a substrate for non–TGF-β receptor kinases (Galliher and Schiemann, 2007), we tested the role of the cytoplasmic domain of TβRII in facilitating the interaction between TβRII and α5. Patch/FRAP analysis of the interactions between myc-TβRII S199, which contains 10 amino acids of the cytoplasmic tail undergoing normal processing and transport to the cell surface (Ehrlich *et al.*, 2001), and integrin α5-RFP (Figure 3Aviii) revealed that the lateral diffusion of integrin α5-RFP was unaffected by immobilization of coexpressed TβRII S199, suggesting loss of TβRII S199 and α5 interaction (Figure 3Aviii). To test whether the TβRII–integrin α5 interaction mediated by the cytoplasmic domain influenced fibrillogenesis in MCF10A cells, we first confirmed the interaction between endogenous TβRII and endogenous α5 using coimmunoprecipitation (Figure 3B). We then examined fibrillogenesis in cells expressing TβRII S199, the complete truncation of the TβRII cytoplasmic domain (TβRII ΔCyto) (Siegel *et al.*, 2003), or control pcDNA. We found that both TβRII ΔCyto– and TβRII S199–expressing MCF10A cells were depleted of fibrils at steady state and failed to mount an increase in FN fibrils in response to TGF-β1 treatment compared with control (pcDNA) cells (Figure 3C). To investigate whether the kinase activity of TβRII, which is necessary for optimal internalization (Anders *et al.*, 1998), is required for TGF-β–induced fibrillogenesis, we used the TβRII point mutant K277R (TβRIIK277R-HA) and tested interaction with integrin α5 using coimmunoprecipitation. We found that, whereas exogenously expressed TβRII-HA in COS7 cells coimmunoprecipitated integrin α5 (Figure 3D), as observed with endogenous receptors in MCF10A cells (Figure 3B), TβRIIK277R was less efficient at immunoprecipitating integrin α5, suggesting a requirement for TβRII kinase activity in the TβRII–integrin α5 interaction. Moreover, similar to the effect of TβRII S199 and TβRII ΔCyto, expressing TβRIIK277R in MCF10A cells resulted in reduced fibrillogenesis in response to TGF-β (Figure 3E). Taken together, these data suggest that the specific, stable interaction between integrin α5 and TβRII requires the cytoplasmic domain and kinase activity of TβRII for TGF-β–mediated fibrillogenesis.

TGF-β increases FN internalization and recycling for fibrillogenesis

The cytoplasmic domain of TβRII, which is critical for TβRII trafficking (Ehrlich *et al.*, 2001; Rechtman *et al.*, 2009), is also required for stable interactions with integrin α5 (Figure 3), which can be bound to FN in early endosome antigen 1 (EEA1)–positive endosomes and multivesicular endosomes (Lobert *et al.*, 2010). Several studies indicated that various forms of exogenously added FN are internalized and localized to distinct cellular compartments in fibroblasts (Sottile and Chandler, 2005; Lobert *et al.*, 2010; Bozavikov *et al.*, 2014). However, whether FN trafficking is directly required for fibrillogenesis is not known. Given the FN synthesis–independent response to TGF-β–induced fibrillogenesis (Figure 1) and the effect of the cytoplasmic domain of TβRII, which is critical for TβRII trafficking (Ehrlich *et al.*, 2001; Penheiter *et al.*, 2002; Mitchell *et al.*, 2004) and now in FN receptor interactions and fibrillogenesis (Figure 3), we tested whether FN trafficking was required for fibrillogenesis in response to TGF-β. To first investigate whether FN is internalized to different extents in the presence of TGF-β, we allowed the uptake of Rh-conjugated fibronectin (Rh-FN; *Materials and Methods*) for 30 min, followed by acid stripping to remove cell surface FN, which we confirmed using TIRF microscopy (Supplemental Figure S2C), to retain only the internalized pool of FN. We observed a twofold increase (*$p < 0.05$) in the internalized pool of Rh-FN between untreated and TGF-β1–treated cells and a threefold increase (**$p < 0.01$) between untreated and TGF-β2–treated cells within 30 min (Figure 4, A and B). Because exogenous FN added to FN-null cells was previously shown to be degraded by the lysosome (Sottile and Chandler, 2005), we tested whether internalized FN in epithelial cells is also degraded in response to a 30-min TGF-β treatment. Lysosomal protein LAMP1 immunolabeling revealed significant FN exclusion (Figure 4C), suggesting that the bulk of internalized FN is not localized to the lysosome upon TGF-β1 and TGF-β2 treatments. In addition, a 6-h lysosomal inhibition with chloroquine (CQ) in TGF-β–treated cells did not significantly increase total FN levels beyond TGF-β–induced FN transcriptional induction (Figure 4D, compare lanes 3 and 4; and 5 and 6), indicating that lysosomal degradation of FN does not occur

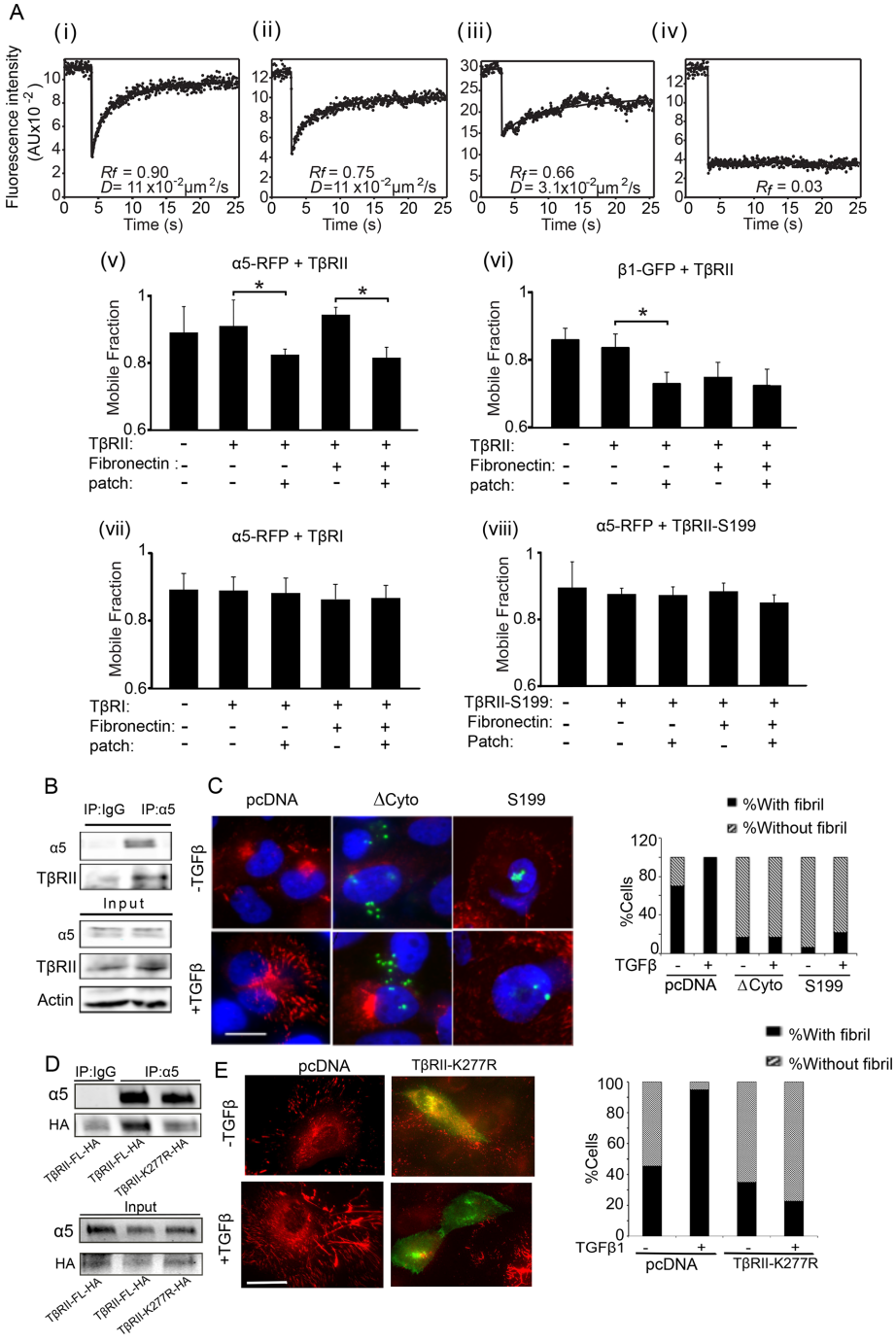

within 6 h of TGF-β1 or TGF-β2 treatment, the time period well within nontranscriptional fibrillogenesis (Figure 1).

Given the TGF-β–induced increase in FN uptake, LAMP1 exclusion of internalized FN, and rapid increase in fibrillogenesis (Figures 1, A and B, and 4, A and C), we asked whether internalized FN could contribute directly to matrix-incorporated (DOC-insoluble) (P) FN. To test this, we used biotinylated FN (FN-biotin) and streptavidin-conjugated secondary antibody to biochemically quantify only the exogenously added FN-biotin (*Materials and Methods*). Because Rh-FN can be internalized within 30 min (Figure 4A), we allowed uptake of FN-biotin for 30 min, followed by repeated washes to remove unbound FN-biotin from the cell surface. The cells were then allowed to recover for 1 h in FN-biotin–free medium in the presence of either serum alone (UN), TGF-β1, or TGF-β2 to test the effect of TGF-β on

FIGURE 3: TβRII's cytoplasmic domain is required for steady-state interactions with integrin α5β1 and fibrillogenesis. (A) COS7 cells were cotransfected with expression vectors encoding myc-TβRII, myc-TβRII S199, or myc-TβRI and integrin α5-RFP or β1-GFP. In control experiments, the integrin construct was replaced by empty vector. At 48 h after transfection, live cells were incubated without or with FN and subjected (or not) to IgG-mediated patching/cross-linking of myc-TβRII or myc-TβRI (*Materials and Methods*), resulting in Alexa 488 (or 546)–labeled myc–TGF-β receptor patched and laterally immobile (iv). In control experiments without cross-linking, the IgG labeling of the myc-TGF-β receptor was replaced by exclusive Fab' labeling (replacing the cross-linking IgGs by their respective Fab' fragments). FRAP studies were conducted on integrin α5–RFP or β1–GFP at 15°C to minimize internalization. The confocal nature of the FRAP experimental setup enabled the measurement of integrin fluorescence recovery exclusively at the plasma membrane (avoiding internal vesicles or ER fluorescence). The laser beam was focused on the upper cell surface and away from cell edges, thus avoiding focal adhesions. Solid lines are the best fit of a nonlinear regression analysis to the lateral diffusion equation (Rechtman *et al.*, 2009). (i) Representative FRAP curve of the lateral diffusion of integrin α5-RFP in a cell coexpressing myc-TβRII (no IgG cross-linking). (ii) A FRAP curve of integrin α5-RFP in a cell coexpressing myc-TβRII immobilized by IgG cross-linking. (iii) A FRAP curve of the lateral diffusion of myc-TβRII. (iv) A FRAP curve of the lateral diffusion of myc-TβRII immobilized by IgG cross-linking. (v–viii) Average R_f values derived from multiple patch/FRAP measurements (coexpressed receptor pairs are indicated above each graph). Because the *D* values were unaffected in all cases (0.1 ± 0.02 µm^2/s), they are not shown. Bars are mean ± SEM of 30–50 measurements in each case. Asterisks indicate significant differences between the R_f values of the pair indicated by brackets (*$p < 0.001$; Student's *t* test). (B) MCF10A cells were immunoprecipitated with integrin α5 antibody or IgG as control and immunoblotted as indicated for endogenous TβRII and integrin α5. Input loading control was actin. (C) MCF10A cells transfected with empty vector or TβRII ΔCyto or TβRII S199 were treated with TGFβ1 (10 ng/ml for 30 min) and coimmunostained using anti-HA (green) to identify transfected cells and anti-FN to endogenous FN (red). Scale bar, 5 µm. Quantitation of percentage of fibril-containing cells (*Materials and Methods*) in the indicated conditions; $N > 200$. (D) COS7 cells transfected for 48 h with indicated TβRII constructs followed by immunoprecipitation with anti-α5 antibody and immunoblotted using either anti-HA or anti-α5 as indicated. (E) MCF10A cells transfected with empty vector or TβRII K277R were treated with TGFβ1 (10 ng/ml for 30 min) and coimmunostained using anti-HA (green) to identify transfected cells and anti-FN to endogenous FN (red). Scale bar, 4 µm. Quantitation of percentage of fibril-containing cells (*Materials and Methods*) in the indicated conditions; $N > 50$.

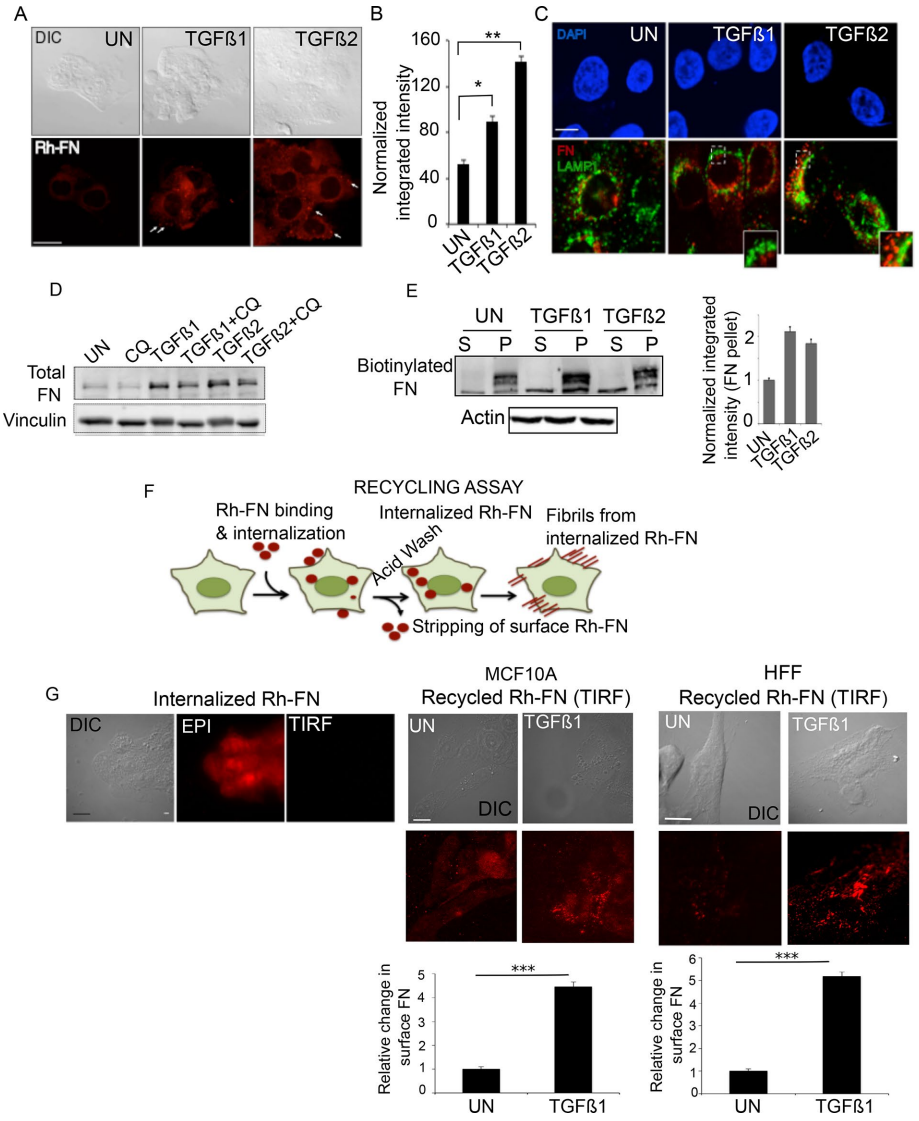

FIGURE 4: TGF-β increases FN internalization and recycling for fibrillogenesis. (A) Rh-FN at 20 µg/ml was added to MCF10A cells either untreated or in the presence of TGF-β1 and TGF-β2 for 30 min, followed by stripping of cell surface Rh-FN (*Materials and Methods*). Representative fluorescence images of Rh-FN. Scale bar, 5 µm. Arrows indicate internalized Rh-FN. (B) Quantification of integrated fluorescence intensity of Rh-FN normalized to cell area from cells in A; $N > 100$/condition. Significance was calculated between untreated samples and TGF-β1– (*$p < 0.05$) and TGF-β2–treated (**$p < 0.01$) samples using the Mann–Whitney *U* test. Data are representative of at least three independent experiments. (C) MCF10A cells treated with TGF-β1/TGF-β2 (10 ng/ml, 30 min) were coimmunostained using anti-LAMP1 and anti-FN; images acquired using confocal microscopy. Scale bar, 5 µm. (D) MCF10A cells were treated with TGF-β1 or TGF-β2 for 6 h with or without 100 µM CQ. Lysates were immunoblotted for total FN. Vinculin was used as loading control. (E) Representative DOC-fractionated biotinylated FN (FN-biotin; *Materials and Methods*) in MCF10A cells. FN-biotin at 20 µg/ml was added to cells for 30 min and washed to remove nonspecific FN-biotin binding on the cell surface. The cells were then reincubated in FN-biotin–free medium for 1 h with or without TGF-β1 or TGF-β2, DOC fractionated into (S) and (P) fractions, and immunoblotted using streptavidin-conjugated IR dye to detect FN-biotin. Actin was used as the loading control for the (S) fraction. Right, quantitation showing fold difference between the amounts of FN-biotin in the DOC-fractionated (P) fraction in untreated and TGF-β1– or TGF-β2–treated cells. Data represent quantitation from two independent experiments. Error bars represent SEM. (F) Schematic of the recycling assay using Rh-FN upon incubation of cells with 20 µg/ml Rh-FN for 30 min at 37°C in the absence of TGF-β1 or TGF-β2. Cells are acid stripped to remove surface-bound Rh-FN (Internalized Rh-FN), followed by reincubation of cells in Rh-FN–free medium at 37°C for 1 h in the presence of TGF-β1 or TGF-β2. (G) Recycling assay as described in F; left, Rh-FN internalized by cells imaged after acid stripping using the Epi illumination and TIRF modes (90-nm penetration depth) as indicated to confirm removal of cell surface Rh-FN. Right, images taken under TIRF mode in either MCF10A or HFF cells, showing the reappearance of surface FN in cells untreated or treated with TGF-β1. Images are representative of at least three independent trials. Scale bar, 5 µm. Quantitation presented below was carried out using the 3D object counter on ImageJ as described in *Materials and Methods* after subtracting background from the cell-free regions. $N = 10$/condition. ***$p < 0.001$.

incorporation of internalized FN-biotin into a DOC-insoluble (P) fraction. DOC fractionation of the soluble (S) and insoluble (P) fractions revealed that, compared with untreated cells, there was a twofold increase in the (P) insoluble fraction after TGF-β1 and TGF-β2 stimulation (compare lanes 2, 4, and 6 in Figure 4E). Because TGF-β treatments were carried out in the absence of additional FN-biotin and exogenous FN can be internalized in the presence of TGF-β (Figure 4, A and B), these data suggest that TGF-β can increase fibrillogenesis by using an internalized pool of FN-biotin that is recycled to form fibrils.

To confirm that the insoluble fraction (P) detected by DOC in the foregoing experiment came from the internalized pool, we carried out a recycling assay (Figure 4F, schematic) using labeled Rh-FN, which can be visualized (Weigert and Donaldson, 2005). Internalization and cell surface removal of Rh-FN was carried out by acid stripping (*Materials and Methods*). Images in the Epi mode versus the TIRF mode confirmed internalized Rh-FN (Figure 4G) because no Rh-FN was observed on TIRF mode (Figure 4G). These results indicate that cells internalized Rh-FN within 30 min, and acid washing of the cells completely depleted surface Rh-FN. To test our prediction from Figure 4E that TGF-β enhanced FN recycling, we incubated acid-stripped cells, which now contained only internalized Rh-FN (Figure 4G, left, MCF10A cells), with media containing serum (UN), TGF-β1, or TGF-β2 (Figure 4G and Supplemental Figure S2D). Compared to untreated cells, TGF-β1 substantially increased the appearance of Rh-FN at the cell surface after 1 h of treatment in MCF10A cells (Figure 4G). This observation was not restricted to epithelial cells because TGF-β1 also induced recycling of FN to the cell surface in HFF cells (Figure 4G, right). Similarly, TGF-β2 also increased Rh-FN recycling (Supplemental Figure S2D). These findings lead us to conclude that TGF-β stimulates internalization and recycling of FN (Figure 4, A and G) for fibrillogenesis.

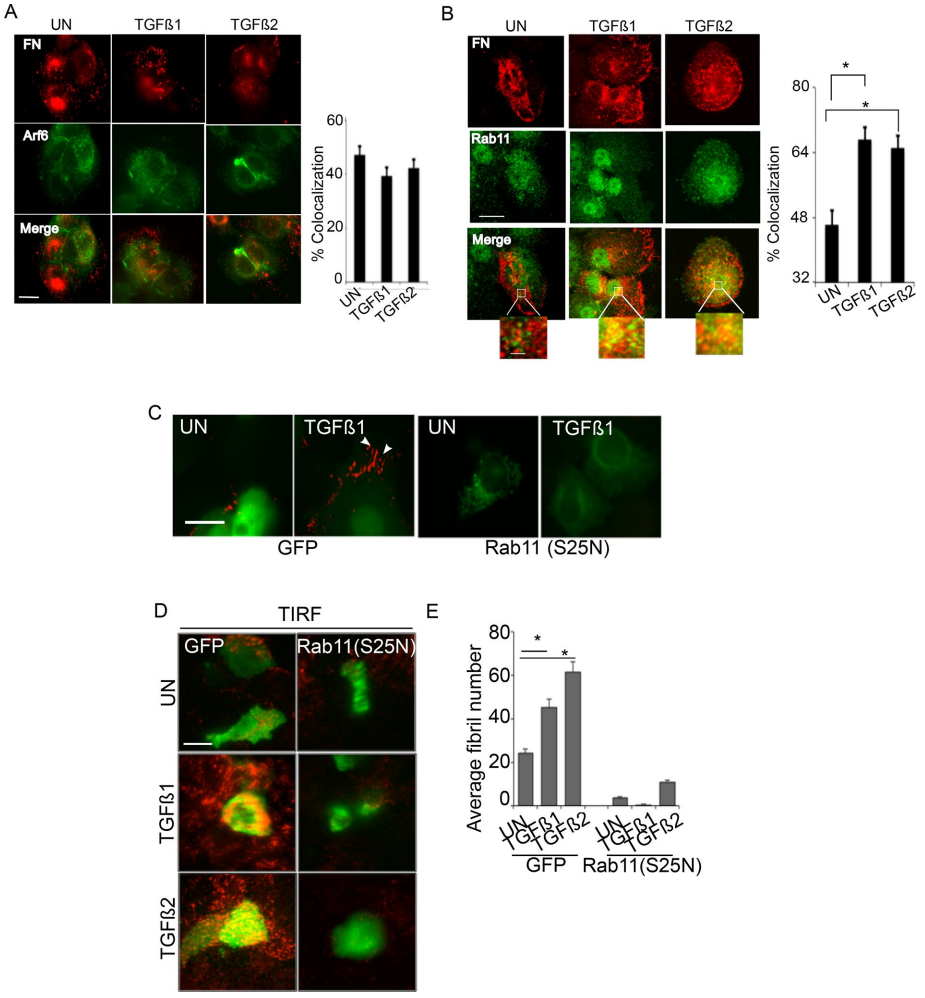

FIGURE 5: FN recycling and fibrillogenesis require the recycling protein Rab11. (A, B) MCF10A cells either untreated (serum alone) or treated with TGF-β1/TGF-β2 (10 ng/ml for 30 min) were coimmunostained using anti-FN and either (A) anti-Arf6 or (B) anti-Rab11 and imaged using confocal microscopy. Scale bar, 5 μm (main image), 1 μm (inset). Percentage colocalization from A and B was determined using the Coloc2 plug-in in ImageJ (*Materials and Methods*) from single *z*-plane between FN and either Arf6 or Rab11 in untreated compared with TGF-β1– or TGF-β2–treated cells. Asterisk indicates significant differences in percentage colocalization ($N > 15$) between untreated compared with TGF-β1– or TGF-β2–treated cells (*$p < 0.001$, *t* test). Images are representative of at least three independent experiments. (C) Recycling assay as described in Figure 4F in the presence of Rh-FN in pEGFP and Rab11 (S25N)-GFP–transfected MCF10A cells. Cells either untreated (UN) or treated with 10 ng/ml TGF-β1 for 30 min were imaged. Only constructs expressing EGFP or Rab11(S25N)-GFP (as monitored by GFP expression) were imaged, and representative images are presented showing abrogated recycling of Rh-FN in Rab11 (S25N) transfectants. Arrowheads indicate fibrils. Scale bar, 2 μm. (D) MCF10A cells were transfected with pEGFP or Rab11 (S25N)-GFP as in C, immunostained using anti-FN after treatments with TGF-β1 or TGF-β2 (10 ng/ml for 30 min), and imaged using TIRF microscopy (penetration depth, 110 nm). Scale bar, 5 μm. (E) Average fibril number/cell analyzed as described in *Materials and Methods* from TIRF images in GFP and Rab11 (S25N) mutants in untreated (UN) cells or cells treated with TGF-β1 or TGF-β2. Fibril lengths were tracked using the NeuronJ plug-in on ImageJ. Asterisk indicates significant differences ($N = 10$ [ANOVA]) in fibril number between untreated GFP transfectants for untreated (UN) cells and cells treated with TGF-β1 or TGF-β2 (*$p < 0.001$).

Fibrillogenesis requires the recycling protein Rab11

Having observed FN recycling in response to TGF-β for fibrillogenesis (Figure 4), we next investigated the recycling pathways required for fibrillogenesis. Arf6 and Rab11 are two components of the major recycling pathways, with Rab11 playing roles in both TβRII and integrin recycling (Mitchell *et al.*, 2004; Kobayashi and Fukuda, 2013). Specifically, Arf6 colocalizes with inactive integrin β1, and Rab11 colocalizes with active integrin β1 and specifically regulates trafficking of the α5β1 heterodimer (Caswell *et al.*, 2007; Arjonen *et al.*, 2012). To test whether FN colocalizes with Rab11 or Arf6 in response to TGF-β, we determined the localization of untreated and TGF-β–induced internalized FN pools with components of the major recycling pathways. We observed no significant colocalization between FN and Arf6 in TGF-β1– and TGF-β2–treated cells compared with untreated cells (Figure 5A). In contrast, both steady-state and TGF-β–treated cells showed FN colocalization with Rab11 (Figure 5B). Moreover, TGF-β1 and TGF-β2 increased colocalization of FN with Rab11 by 1.7- and 1.4-fold, respectively (*$p < 0.001$; Figure 5B). Not all available FN was associated with Rab11. It is therefore possible that a fraction of internalized FN does not colocalize with Rab11 and may undergo degradation (Sottile and Chandler, 2005; Lobert *et al.*, 2010) or recycle through alternate modes, including Rab4 (Roberts *et al.*, 2001).

Owing to the observed colocalization of FN with Rab11 in response to TGF-β (Figure 5B), we tested whether Rab11 was involved in FN recycling for fibrils. We carried out the recycling assay (as described in Figure 4F; Weigert and Donaldson, 2005) in cells transfected with either GFP or Rab11-S25N, a dominant-negative Rab11 mutant that fails to recycle cargo proteins to the plasma membrane (Ren *et al.*, 1998). Rh-FN was added to the cells for uptake, acid washed to remove surface bound Rh-FN, and allowed to recover in medium containing either serum or TGF-β as described in the schematic in Figure 4F, and the appearance of the fibrils was determined. In GFP-transfected cells, we observed an increase in short Rh-FN fibrils in response to TGF-β (Figure 5C). However, in the Rab11-S25N transfectants, we observed no appearance of Rh-FN fibrils (Figure 5C), demonstrating that Rab11 function is required for TGF-β–induced rapid FN fibrillogenesis. To confirm whether Rab11-S25N abolished cell surface fractions of FN fibrils as seen in Figure 5C, we used TIRF imaging. We consistently observed significantly fewer cell surface fibrils in Rab11-S25N transfectants than in control cells (*$p < 0.001$; Figure 5, D and E). These data collectively demonstrate that FN uses the recycling protein Rab11 to return to the surface for enhanced fibrillogenesis.

DISCUSSION

In this study, we demonstrate a nontranscriptional mechanism by which TGF-β induces fibrillogenesis via enhanced FN trafficking. We find rapid fibrillogenesis in response to TGF-β1 and TGF-β2 in both

fibroblast and epithelial cells. We accomplished this by measuring incorporation of both exogenous and cell-produced FN into a DOC-insoluble matrix and visualizing at the cell surface using immunolabeling of FN and TIRF microscopy. Using the 49-mer FUD peptide to bind N-terminal sites on FN (Tomasini-Johansson *et al.*, 2006), we efficiently blocked incorporation of FN into the DOC-insoluble pool and fibril appearance induced by TGF-β (Figure 1), confirming the fibrillar nature of the rapid TGF-β response. TGF-β plays dominant roles in regulating cell motility and EMT (Wendt *et al.*, 2012; Morrison *et al.*, 2013), and we find fibrillogenesis in cells undergoing chemotactic migration (Figure 1J). TGF-β is also a robust inducer of cell motility and invasion in many cell types, including epithelial cells that do not produce significant amounts of fibronectin. However, TGF-β–induced cell migration is indeed repressed by the fibrillogenesis-blocking FUD peptide. Because our data suggest that TGF-β–induced early fibrillogenesis uses recycled FN pools (Figures 4 and5) and does not require new protein synthesis (Figure 1D), we speculate that such rapid changes in the ECM that precede a transcriptional response are likely to be an important mechanism for triggering mechanical signals that can potentiate and sustain TGF-β responses.

We also discovered that TGF-β–induced fibrillogenesis requires the type II TGF-β receptor, using multiple cell models, including isogenic mink lung cells lacking the TβRII receptor (Laiho *et al.*, 1990; Figure 2, B and C), and receptor silencing (Figure 2, D–G) in epithelial cells. We also find that TβRII's cytoplasmic domain is required to maintain steady-state levels of FN fibrils and is critical for TGF-β induced fibrillogenesis (Figures 2 and 3). Such a requirement may stem from either the kinase activity of the receptor or loss of interactions with the FN receptor integrin α5β1 mediated via TβRII's cytoplasmic domain. Indeed, the interaction between integrin α5 and TβRII is reduced in the K277R mutant of TβRII (Figure 3). TGF-β can mediate both SMAD and non-SMAD responses, with TβRII phosphorylation by non–TGF-β receptor kinases such as Src being critical for bridging TGF-β and TβRII to non-SMAD mitogen-activated protein kinase activation (Feng and Derynck, 1996; Derynck and Zhang, 2003; Galliher and Schiemann, 2007). Our data indicate that SMAD pathways are not involved in the rapid fibrillogenesis response due to the minor role of TβRI (Figures 2 and 3). These findings indicate that the initial fibrillogenesis response is a novel non-SMAD outcome and could precede or be required for a longer-term SMAD response to maintain fibrillogenesis.

Our data from coimmunoprecipitation and PATCH/FRAP experiments show stable cell surface interactions between TβRII and integrins α5 and β1. Whether the activation state of the integrin α5β1 heterodimer dictates the TβRII-integrin interaction remains to be determined. The interaction between TβRII and integrin α5 appears to be only marginally increased by FN (Figure 3), suggesting steady-state complexes that are likely to result in constitutive trafficking of the bound ECM ligand. On the other hand, FN addition was able to immobilize a subpopulation of integrin β1 without cross-linking of TβRII. This may reflect fibronectin-mediated clustering of integrin β1 that links it with the cytoskeleton and thus induces partial immobilization (McKeown-Longo and Mosher, 1984; Bhatia *et al.*, 1999). Whereas TGF-β receptor and integrin trafficking have been separately examined previously (Yao *et al.*, 2002; Caswell *et al.*, 2009), there is limited knowledge on whether ECM components traffic along with the receptors. Both integrin α5β1 and TβRII undergo constitutive endocytosis and recycling, with specific endocytosis and recycling routes influencing either receptor signaling or receptor turnover (Di Guglielmo *et al.*, 2003; Lobert *et al.*, 2010; Arjonen *et al.*, 2012). Hence it is likely that ECM deposition may be coordinated/coupled to receptor trafficking. Integrins have, in turn, been shown to dictate ECM protein endocytosis and turnover (Panetti and McKeown-Longo, 1993; Shi and Sottile, 2008). However, evidence on the regulation of ECM traffic by growth factors and its effect on ECM remodeling is scarce. We find that FN is internalized and recycled in the presence of TGF-β in a TβRII-dependent manner to be reused to form fibrils (Figure 4). Similarly, our patch/FRAP experiments to measure interactions between the trafficking mutant TβRII S199 and integrin α5 demonstrate loss of the stable interaction between the two receptors (Figure 3) and less robust fibrils in the TβRII S199 transfectants (Figure 3). Thus fibrillogenesis requires the TβRII–integrin α5β1 interaction. It is likely that the dominant-negative effects of TβRII S199 or TβRII ΔCyto affect endogenous TβRII receptor and/or integrin trafficking and ultimately disrupt fibrillogenesis.

It was shown previously that fibronectin, along with integrin α5, internalizes and localizes to the lumen of multivesicular endosomes with EEA1, a prerequisite for integrin sorting and recycling (Lobert *et al.*, 2010). Our data are the first demonstration of FN recycling after internalization (Figure 4). Whether TGF-β–induced FN trafficking and recycling occur concomitantly with active or inactive integrins, with or without TGF-β receptors, is the focus of our ongoing studies and will include analyzing the role of the catalytically active from of TβRII (TβRIIP525L; Carcamo *et al.*, 1995), which is also signaling deficient and has altered endocytosis and recycling in a cell type–dependent manner (Anders *et al.*, 1998; Dore *et al.*, 1998, 2001). We anticipate that these future studies will provide insights into TGF-β receptor– integrin trafficking and their effect on matrix remodeling.

Our observations of FN localization with Rab11, which is increased in the presence of TGF-β (Figure 5) and is required for fibrillogenesis (Figure 5), suggest Rab11 as a recycling route for FN. However, we cannot completely rule out that a pool of FN may recycle via Rab4, which has been shown to carry αvβ3 (Roberts *et al.*, 2001). Prior published routes on TβRII and integrin α5β1 trafficking showing that 1) TGF-β receptor internalized into early endosomes can recycle via Rab 11(Penheiter *et al.*, 2002; Mitchell *et al.*, 2004) and 2) integrin internalization via Rab5 endosomes can be recycled via Rab 11 (Pellinen and Ivaska, 2006; Arjonen *et al.*, 2012), together with 3) our findings of FN recycling via Rab11 (Figure 5), indicate that a pool of FN recycles with integrin in a Rab11-dependent manner, possibly along with TβRII. It is also likely that FN, integrin, and TβRII internalize into early endosomes concomitantly in response to TGF-β in either a clathrin/dynamin- or caveolin-dependent way. This is consistent with observations that endocytic trafficking via clathrin-mediated endocytosis shifts the fate of TGF-β receptors from lysosomal degradation to prolonged signaling (Penheiter *et al.*, 2002; Mitchell *et al.*, 2004).

In conclusion, we provided new insights into growth factor–controlled fibrillogenesis and showed, for the first time, that FN can be rapidly channeled into FN fibrils from available sources of FN within 30 min. Whether this mechanism can complement transcriptionally induced FN function or exhibit distinct cellular functions remains to be examined. We anticipate that this nontranscriptional source of fibrillogenesis might play a significant role in rapid ECM remodeling and reinforcement of growth factor responses, particularly during events requiring precise spatial control of fibrillogenesis, with implications for cell migration, wound repair, and fibrosis.

MATERIALS AND METHODS

Cell line and culture conditions

Nontumorigenic MCF10A breast epithelial cells were obtained from the American Type Culture Collection and cultured in DMEM/F12 (1:1) with 5% horse serum, epidermal growth factor (20 ng/ml),

hydrocortisone (0.5 mg/ml), cholera toxin (100 ng/ml), and insulin (10 μg/ml). Human foreskin fibroblasts, COS7 cells, and mink lung epithelial cells MV1Lu, DR, and R1b were cultured in DMEM supplemented with 10% fetal bovine serum (FBS), and glutamine. Cell lines were maintained in 37°C humidified incubator buffered with 5% CO_2.

Antibodies, reagents, and plasmids

Antibodies to FN (sc8422) and TβRII (sc220) were from Santa Cruz Biotechnology. Rabbit hemagglutinin (HA) tag (C29F4), integrin α5 (4705S), and LAMP1 (D2D11) were from Cell Signaling Technology. The 9E10 mouse ascites against the myc tag (Evan *et al.*, 1985) was from Covance Research Products (Denver, PA). Anti-myc IgG and monovalent Fab' fragments were prepared from the 9E10 ascites as described (Henis *et al.*, 1994). Alexa Fluor 488–goat anti-mouse IgG and Alexa Fluor 546–goat anti mouse F(ab')$_2$ were from Invitrogen-Molecular Probes (Eugene, OR); fluorescent F(ab')$_2$ was converted to Fab' as described (Gilboa *et al.*, 1998). Rab11 (71-5300) was from Life Technologies, and Integrin α5 (P1D6) for immunoprecipitation was from the Developmental Studies Hybridoma Bank (University of Iowa, Iowa City, IA). Vinculin (CP74) was from Calbiochem, and β-actin (A2228) was from Sigma-Aldrich. Ligands TGF-β and FN were from R&D systems. Lipofectamine 2000 (11668019) was from Life Technologies. Nocodazole (358240100) was from Fisher, and CHX (94271-5G) was from Amresco. Rh-FN (FNR01 and custom FNR04) and biotinylated FN (FNR03-A) were from Cytoskeleton. Propidium iodide (537059) was from Calbiochem. Plasmids expressing GFP-Rab11S25N (Choudhury *et al.*, 2002; plasmid ID 12678), HA-tagged dynamin K44A (Song *et al.*, 2004; plasmid ID 34683) and HA-tagged TβRII-ΔCyto (Siegel *et al.*, 2003; plasmid ID 14051) were obtained from Addgene. The expression vectors encoding myc-tagged human TβRII, myc-TβRII S199, and myc-TβRI (in pcDNA3) were previously described (Ehrlich *et al.*, 2001; Yao *et al.*, 2002). Integrin α5-RFP and integrin β1-GFP were constructed based on commercially obtained clones of the human receptors (OriGene); the coding regions were inserted N-terminally to monomeric RFP (Ehrlich *et al.*, 2004) or enhanced GFP (EGFP) Clontech) by PCR.

TβRII knockdown

Two different Mission shRNA sequences from Sigma-Aldrich were used to knock down TβRII levels. shTβRII-1, 5'-CCGGATGGAAGACTTTAAGGTATTTCTCGAGAAATACCTTAAAGTCTCCATTTTTTTG-3'; and shTβRII-2, 5'-CCGGCAATAACAAAGGCGCAAATAACTCGAGTTATTTGCGCCTTTGTTATTGTTTTTTG-3'.

Deoxycholate fractionation of FN

Deoxycholate fractionation of FN was carried out according to a previously published protocol (Sechler *et al.*, 1996). Briefly, cells were washed in ice-cold phosphate-buffered saline (PBS), followed by lysate preparation in buffer containing 2% deoxycholate and 0.02 M Tris-HCl, pH 8.8, supplemented with 2 mM phenylmethylsulfonyl fluoride, 2 mM EDTA, 2 mM iodoacetic acid, and 2 mM *N*-ethylmalemide. Lysis was carried out by passing the lysate through a 23-gauge syringe needle several times, followed by incubation on a rotor wheel for 30 min. The lysates were centrifuged at 15,000 rpm for 30 min, and the supernatant was transferred to another tube as the soluble fraction. The pellet/insoluble fraction was resuspended in SDS lysis buffer containing 1% SDS, 25 mM Tris-HCl, pH 8.0, and protease inhibitors. Lysates containing SDS were heated for 1 min at 95°C. In deoxycholate fractionation experiments, which involve the comparison of ratios between samples, the entire pellet fraction was loaded onto the gel, and 10% of the soluble fraction was loaded alongside. This allows the internal comparison of FN ratios within the sample and between samples.

Transwell migration assay

Fifty thousand MCF10A cells in serum-free medium containing Rh-FN were seeded in the upper chamber of a Transwell filter. The filter was coated on both sides with 10 μg/ml FN before the migration assay, and cells were allowed to migrate toward the lower chamber containing medium with 10% FBS (chemotactic gradient) for 6 h at 37°C. Cells on the upper surface of the filter were removed, and only cells on the lower face of the filter were fixed in 4% paraformaldehyde and mounted using mount medium containing 4'6-diamidino-2-phenylindole (DAPI).

Flow cytometry

Approximately 1 million cells were fixed in 70% ethanol and washed in ice-cold 1% bovine serum albumin (BSA) in PBS. The cell pellet was resuspended in 2 ml of ice-cold PBS and fixed in 5 ml of 100% ethanol added dropwise to keep the final ethanol concentration at 70%. After fixing overnight at 20°C, the fixative was removed and the samples labeled with 10 μg/ml propidium iodide in 0.1% Triton X-100 with RNase and incubated for 20 min at room temperature. The samples were filtered and run on a BD LASRII Flow Cytometer.

Immunofluorescence and transfection

Cells were fixed in 4% paraformaldehyde, permeabilized in 0.3% Triton X-100, and blocked with 1% BSA in PBS. Primary antibody (1:200) incubation for 1 h was followed by 30 min of incubation with Dylight 800 conjugate (5151 Cell Signaling Technology). After washing, cells were stained with DAPI (Roche). Immunostaining of FN (1:100) to visualize fibrils was carried out by fixing in 4% paraformaldehyde and permeabilized in 0.1% Triton X-100 for 1 min at 4°C. Immunofluorescence imaging and *z*-stacking were performed using a Zeiss LSM700 confocal microscope. Transfection using Lipofectamine 2000 was carried out according to manufacturer's instructions.

Microscopy

TIRF images were captured using a Leica AM inverted motorized microscope equipped with a Hamamatsu ImagEM back-thinned electron-multiplying cooled charge-coupled device camera. FN fibrils were imaged using the TIRF module at laser penetration depth of 110 or 90 nm as indicated (Leica HCX Plan Apo objective). Immunofluorescence imaging and *z*-stacking for colocalization analyses were performed using a Zeiss LSM700 confocal microscope. Wide-field immunofluorescence images were imaged using the Olympus IX81 microscope connected to an Olympus 1XZ-UCB camera.

Statistical analyses and quantification

ImageJ was used to quantify pixel intensities of immunoblots. In Figure 4A, integrated pixel intensities were measured relative to surface area of the cells, and the data were acquired setting a constant threshold of 43 for all the treatment conditions used. Because intensity values represented continuous data points, we used the nonparametric Mann-Whitney *U* test to calculate *p* value. Data are representative of multiple experiments. Colocalization analyses in Figure 5 were calculated from single *z*-planes from different regions of interest (ROIs) at a Coates significance of 1 and computed using the Coloc2 plug-in in ImageJ. Student's *t* test was used to calculate *p* value. At least 50 different ROIs were included in a single analysis. Plots in Figures 1, 2, and 5 were constructed

based on the observation that a fibril is considered a single track of at least 3 µm in length (Coussen *et al.*, 2002; Lutz *et al.*, 2011). A fibronectin trimer and a pentamer have been shown to form fibril-like structures. The pentamer has a length of 90–100 nm (Coussen *et al.*, 2002). Because the resolution of our microscope has a 200-nm limit, this made it unreliable to optically zoom into images to carry out quantification and analyses. A 3-µm cutoff was the smallest length that resembled a fibril, as opposed to an aggregate of fibronectin as previously described (Lutz *et al.*, 2011). Cells containing fibrils of such threshold lengths were counted as "with fibril" using the Neuron J plug-in on ImageJ and plotted. Analysis of variance (ANOVA) with Holm–Sidak test was used to calculate *p* values. Data are representative of multiple experiments. Quantitation in Figure 4G was carried out using the three-dimensional (3D) object counter on ImageJ. We set a grid on the TIRF images and introduced a size filter of >30 voxels. We picked the size cut-off based on background Rh signal noise, which was completely filtered out at >30 in cell free samples. We randomly analyzed 20 ROIs for 10 cells/condition.

Error bars in all experiments represent SEM.

Rhodamine FN–uptake experiments

This protocol is a modification to the published protocol (Weigert and Donaldson, 2005). Before measuring the uptake and recycling of Rh-FN, we serum starved cells for 6 h in medium containing 20 µg/ml CHX. To measure uptake, the cells were incubated in 20 µg/ml Rh-FN in serum-free medium for 30 min at 37°C to allow incorporation. To measure uptake, the coverslip was repeatedly washed in PBS, followed by two 30-s washes in acid stripping solution containing 0.5 M NaCl and 0.09 M acetic acid. The coverslips were rinsed again in ice-cold PBS and fixed for immunostaining. The efficiency of the acid stripping was determined using TIRF microscopy. To measure recycling, the acid-stripped coverslips were returned to a 37°C incubator in medium containing serum and growth factors. After 1 h, the coverslips were repeatedly rinsed in PBS and fixed for immunostaining and visualization. Resurfacing of Rh-FN as measured by TIRF microscopy (penetration depth, 90 nm) was a measure of recycled FN, which was detectable only on the TIRF mode.

Biotinylation assay to measure recycled FN

Before biotinylation, cells were serum starved for 2 h and then incubated with 20 µg/ml biotinylated FN (noncleavable) for 30 min at 37°C in serum-free medium (steady state). The cells were repeatedly washed in PBS and allowed to recover in biotin-FN free medium for 1 h at 37°C with or without 10 ng/ml TGF-β1 or TGF-β2. The lysates were DOC extracted into soluble (S) and insoluble (pellet [P]) fractions and immunoblotted using streptavidin-conjugated IR Dye (926-32230; Li-Cor).

FRAP and patch/FRAP

FRAP and patch/FRAP were performed essentially as described previously (Henis *et al.*, 1990; Rechtman *et al.*, 2009). Briefly, at 48 h posttransfection, COS7 cells transfected with myc-TβRII, myc-TβRII S199, or myc-TβRI together with integrin α5-RFP or integrin β1-GFP were serum starved (30 min, 37°C), washed with cold Hanks' balanced salt solution (HBSS) supplemented with 20 mM 4-(2-hydroxyethyl)-1-piperazineethanesulfonic acid (HEPES; pH 7.2) and 2% BSA (Sigma-Aldrich), and blocked with normal goat γ-globulin (200 µg/ml, 30 min, 4°C). They were then labeled successively at 4°C (to avoid internalization and enable exclusive cell surface labeling) in HBSS/HEPES/BSA (45-min incubations) with 1) anti-myc IgG (40 µg/ml) and 2) Alexa Fluor 488 (or 546)–IgG goat anti-mouse (40 µg/ml). This protocol results in the myc-tagged receptors cross-linking and immobilization by IgGs. In control experiments in which myc-TβRII or myc-TβRI was not cross-linked, the foregoing IgGs were replaced by equivalent monovalent Fab' fragments. The integrin α5–RFP (or integrin β1–GFP) in cells treated as described were subjected to FRAP and patch/FRAP studies as described earlier (Rechtman *et al.*, 2009). The FRAP measurements were conducted at 15°C, replacing samples within 20 min to minimize internalization during the measurement. An argon-ion laser beam (Innova 70C; Coherent, Santa Clara, CA) was focused through a fluorescence microscope (Axioimager. D1; Carl Zeiss MicroImaging, Jena, Germany) to a Gaussian spot of 0.77 ± 0.03 µm (Plan Apochromat 63×/1.4 numerical aperture oil-immersion objective). After a brief measurement at monitoring intensity (528.7 nm and 1 µW for RFP and 488 nm at similar conditions for GFP), a 5-mW pulse (20 ms) bleached 60–75% of the fluorescence in the illuminated region, and fluorescence recovery was followed by the monitoring beam. Values of D and R_f were extracted from the FRAP curves by nonlinear regression analysis, fitting to a lateral diffusion process (Rechtman *et al.*, 2009) Patch/FRAP studies were performed similarly, except that IgG-mediated cross-linking/patching of a myc-tagged TGF-β receptor (described earlier) preceded the measurement (Rechtman *et al.*, 2009). This enables us to determine the effect of immobilizing one receptor type on the lateral diffusion of the coexpressed fluorescent protein, allowing identification of complex formation between them and distinction between transient and stable interactions (Henis *et al.*, 1990; Rechtman *et al.*, 2009).

ACKNOWLEDGMENTS

We thank Gary Schools (Microscopy Core Facility, University of South Carolina), Pratik Patel, and Alejandro Frank for technical help. We are also extremely grateful to Jane Sottile (University of Rochester) for generously sharing the FUD and control peptide and Jean Schwarzbauer (Princeton University) and Vinay Swaminathan (National Institutes of Health) for helpful discussions. This work was funded in part by Ovarian Cancer Research Fund Grant 258785 to K.M., National Institutes of Health Grant P20 GM109091 to K.M., and Grant 148/13 from the Israel Science Foundation to Y.I.H. Y.I.H. holds the Zalman Weinberg Chair in Cell Biology.

REFERENCES

Abraham LC, Vorrasi J, Kaplan DL (2004). Impact of collagen structure on matrix trafficking by human fibroblasts. J Biomed Mater Res A 70, 39–48.

Allen-Hoffmann BL, Crankshaw CL, Mosher DF (1988). Transforming growth factor beta increases cell surface binding and assembly of exogenous (plasma) fibronectin by normal human fibroblasts. Mol Cell Biol 8, 4234–4242.

Anders RA, Dore JJ Jr, Arline SL, Garamszegi N, Leof EB (1998). Differential requirement for type I and type II transforming growth factor beta receptor kinase activity in ligand-mediated receptor endocytosis. J Biol Chem 273, 23118–23125.

Arjonen A, Alanko J, Veltel S, Ivaska J (2012). Distinct recycling of active and inactive beta1 integrins. Traffic 13, 610–625.

Bhatia R, Munthe HA, Verfaillie CM (1999). Role of abnormal integrin-cytoskeletal interactions in impaired beta1 integrin function in chronic myelogenous leukemia hematopoietic progenitors. Exp Hematol 27, 1384–1396.

Bhowmick NA, Zent R, Ghiassi M, McDonnell M, Moses HL (2001). Integrin beta 1 signaling is necessary for transforming growth factor-beta activation of p38MAPK and epithelial plasticity. J Biol Chem 276, 46707–46713.

Biname F, Lassus P, Hibner U (2008). Transforming growth factor beta controls the directional migration of hepatocyte cohorts by modulating their adhesion to fibronectin. Mol Biol Cell 19, 945–956.

Bortell R, Owen TA, Ignotz R, Stein GS, Stein JL (1994). TGF beta 1 prevents the down-regulation of type I procollagen, fibronectin, and TGF beta 1 gene expression associated with 3T3-L1 pre-adipocyte differentiation. J Cell Biochem 54, 256–263.

Boyd FT, Massague J (1989). Transforming growth factor-beta inhibition of epithelial cell proliferation linked to the expression of a 53-kDa membrane receptor. J Biol Chem 264, 2272–2278.

Bozavikov P, Rajshankar D, Lee W, McCulloch CA (2014). Particle size influences fibronectin internalization and degradation by fibroblasts. Exp Cell Res 328, 172–185.

Carcamo J, Zentella A, Massague J (1995). Disruption of transforming growth factor beta signaling by a mutation that prevents transphosphorylation within the receptor complex. Mol Cell Biol 15, 1573–1581.

Caswell PT, Spence HJ, Parsons M, White DP, Clark K, Cheng KW, Mills GB, Humphries MJ, Messent AJ, Anderson KI, *et al*. (2007). Rab25 associates with alpha5beta1 integrin to promote invasive migration in 3D microenvironments. Dev Cell 13, 496–510.

Caswell PT, Vadrevu S, Norman JC (2009). Integrins: masters and slaves of endocytic transport. Nat Rev Mol Cell Biol 10, 843–853.

Chiang HY, Korshunov VA, Serour A, Shi F, Sottile J (2009). Fibronectin is an important regulator of flow-induced vascular remodeling. Arterioscler Thromb Vasc Biol 29, 1074–1079.

Choudhury A, Dominguez M, Puri V, Sharma DK, Narita K, Wheatley CL, Marks DL, Pagano RE (2002). Rab proteins mediate Golgi transport of caveola-internalized glycosphingolipids and correct lipid trafficking in Niemann-Pick C cells. J Clin Invest 109, 1541–1550.

Clark K, Pankov R, Travis MA, Askari JA, Mould AP, Craig SE, Newham P, Yamada KM, Humphries MJ (2005). A specific alpha5beta1-integrin conformation promotes directional integrin translocation and fibronectin matrix formation. J Cell Sci 118, 291–300.

Coussen F, Choquet D, Sheetz MP, Erickson HP (2002). Trimers of the fibronectin cell adhesion domain localize to actin filament bundles and undergo rearward translocation. J Cell Sci 115, 2581–2590.

Daly AC, Randall RA, Hill CS (2008). Transforming growth factor beta-induced Smad1/5 phosphorylation in epithelial cells is mediated by novel receptor complexes and is essential for anchorage-independent growth. Mol Cell Biol 28, 6889–6902.

Danen EH, Sonnenberg A (2003). Integrins in regulation of tissue development and function. J Pathol 201, 632–641.

Danen EH, Sonneveld P, Brakebusch C, Fassler R, Sonnenberg A (2002). The fibronectin-binding integrins alpha5beta1 and alphavbeta3 differentially modulate RhoA-GTP loading, organization of cell matrix adhesions, and fibronectin fibrillogenesis. J Cell Biol 159, 1071–1086.

de Caestecker M (2004). The transforming growth factor-beta superfamily of receptors. Cytokine Growth Factor Rev 15, 1–11.

Derynck R, Zhang YE (2003). Smad-dependent and Smad-independent pathways in TGF-beta family signalling. Nature 425, 577–584.

Di Guglielmo GM, Le Roy C, Goodfellow AF, Wrana JL (2003). Distinct endocytic pathways regulate TGF-beta receptor signalling and turnover. Nat Cell Biol 5, 410–421.

Dore JJ Jr, Edens M, Garamszegi N, Leof EB (1998). Heteromeric and homomeric transforming growth factor-beta receptors show distinct signaling and endocytic responses in epithelial cells. J Biol Chem 273, 31770–31777.

Dore JJ Jr, Yao D, Edens M, Garamszegi N, Sholl EL, Leof EB (2001). Mechanisms of transforming growth factor-beta receptor endocytosis and intracellular sorting differ between fibroblasts and epithelial cells. Mol Biol Cell 12, 675–684.

Ehrlich M, Boll W, Van Oijen A, Hariharan R, Chandran K, Nibert ML, Kirchhausen T (2004). Endocytosis by random initiation and stabilization of clathrin-coated pits. Cell 118, 591–605.

Ehrlich M, Shmuely A, Henis YI (2001). A single internalization signal from the di-leucine family is critical for constitutive endocytosis of the type II TGF-beta receptor. J Cell Sci 114, 1777–1786.

Eisenberg S, Beckett AJ, Prior IA, Dekker FJ, Hedberg C, Waldmann H, Ehrlich M, Henis YI (2011). Raft protein clustering alters N-Ras membrane interactions and activation pattern. Mol Cell Biol 31, 3938–3952.

Erickson HP, Carrell N, McDonagh J (1981). Fibronectin molecule visualized in electron microscopy: a long, thin, flexible strand. J Cell Biol 91, 673–678.

Erickson HP, Carrell NA (1983). Fibronectin in extended and compact conformations. Electron microscopy and sedimentation analysis. J Biol Chem 258, 14539–14544.

Evan GI, Lewis GK, Ramsay G, Bishop JM (1985). Isolation of monoclonal antibodies specific for human c-myc proto-oncogene product. Mol Cell Biol 5, 3610–3616.

Feng XH, Derynck R (1996). Ligand-independent activation of transforming growth factor (TGF) beta signaling pathways by heteromeric cytoplasmic domains of TGF-beta receptors. J Biol Chem 271, 13123–13129.

Galliher AJ, Schiemann WP (2006). Beta3 integrin and Src facilitate transforming growth factor-beta mediated induction of epithelial-mesenchymal transition in mammary epithelial cells. Breast Cancer Res 8, R42.

Galliher AJ, Schiemann WP (2007). Src phosphorylates Tyr284 in TGF-beta type II receptor and regulates TGF-beta stimulation of p38 MAPK during breast cancer cell proliferation and invasion. Cancer Res 67, 3752–3758.

Galliher-Beckley AJ, Schiemann WP (2008). Grb2 binding to Tyr284 in TbetaR-II is essential for mammary tumor growth and metastasis stimulated by TGF-beta. Carcinogenesis 29, 244–251.

Garamszegi N, Garamszegi SP, Samavarchi-Tehrani P, Walford E, Schneiderbauer MM, Wrana JL, Scully SP (2010). Extracellular matrix-induced transforming growth factor-beta receptor signaling dynamics. Oncogene 29, 2368–2380.

Gilboa L, Wells RG, Lodish HF, Henis YI (1998). Oligomeric structure of type I and type II transforming growth factor beta receptors: homodimers form in the ER and persist at the plasma membrane. J Cell Biol 140, 767–777.

Henis YI, Katzir Z, Shia MA, Lodish HF (1990). Oligomeric structure of the human asialoglycoprotein receptor: nature and stoichiometry of mutual complexes containing H1 and H2 polypeptides assessed by fluorescence photobleaching recovery. J Cell Biol 111, 1409–1418.

Henis YI, Moustakas A, Lin HY, Lodish HF (1994). The types II and III transforming growth factor-beta receptors form homo-oligomers. J Cell Biol 126, 139–154.

Hocevar BA, Brown TL, Howe PH (1999). TGF-beta induces fibronectin synthesis through a c-Jun N-terminal kinase-dependent, Smad4-independent pathway. EMBO J 18, 1345–1356.

Hocevar BA, Howe PH (2000). Analysis of TGF-beta-mediated synthesis of extracellular matrix components. Methods Mol Biol 142, 55–65.

Huck L, Pontier SM, Zuo DM, Muller WJ (2010). beta1-integrin is dispensable for the induction of ErbB2 mammary tumors but plays a critical role in the metastatic phase of tumor progression. Proc Natl Acad Sci USA 107, 15559–15564.

Ignotz RA, Massague J (1986). Transforming growth factor-beta stimulates the expression of fibronectin and collagen and their incorporation into the extracellular matrix. J Biol Chem 261, 4337–4345.

Kobayashi H, Fukuda M (2013). Arf6, Rab11 and transferrin receptor define distinct populations of recycling endosomes. Commun Integr Biol 6, e25036.

Laiho M, Weis MB, Massague J (1990). Concomitant loss of transforming growth factor (TGF)-beta receptor types I and II in TGF-beta-resistant cell mutants implicates both receptor types in signal transduction. J Biol Chem 265, 18518–18524.

Lobert VH, Brech A, Pedersen NM, Wesche J, Oppelt A, Malerod L, Stenmark H (2010). Ubiquitination of alpha 5 beta 1 integrin controls fibroblast migration through lysosomal degradation of fibronectin-integrin complexes. Dev Cell 19, 148–159.

Lotz MM, Burdsal CA, Erickson HP, McClay DR (1989). Cell adhesion to fibronectin and tenascin: quantitative measurements of initial binding and subsequent strengthening response. J Cell Biol 109, 1795–1805.

Lutz R, Pataky K, Gadhari N, Marelli M, Brugger J, Chiquet M (2011). Nanostenciled RGD-gold patterns that inhibit focal contact maturation induce lamellipodia formation in fibroblasts. PLoS One 6, e25459.

Mao Y, Schwarzbauer JE (2005). Fibronectin fibrillogenesis, a cell-mediated matrix assembly process. Matrix Biol 24, 389–399.

Massague J (2012). TGFbeta signalling in context. Nat Rev Mol Cell Biol 13, 616–630.

Massague J, Heino J, Laiho M (1991). Mechanisms in TGF-beta action. Ciba Found Symp 157, 51–59, discussion 59–65.

McKeown-Longo PJ, Mosher DF (1984). Mechanism of formation of disulfide-bonded multimers of plasma fibronectin in cell layers of cultured human fibroblasts. J Biol Chem 259, 12210–12215.

Mitchell H, Choudhury A, Pagano RE, Leof EB (2004). Ligand-dependent and -independent transforming growth factor-beta receptor recycling regulated by clathrin-mediated endocytosis and Rab11. Mol Biol Cell 15, 4166–4178.

Morrison CD, Parvani JG, Schiemann WP (2013). The relevance of the TGF-beta Paradox to EMT-MET programs. Cancer Lett 341, 30–40.

Murphy SJ, Shapira KE, Henis YI, Leof EB (2007). A unique element in the cytoplasmic tail of the type II transforming growth factor-beta receptor controls basolateral delivery. Mol Biol Cell 18, 3788–3799.

Mythreye K, Knelson EH, Gatza CE, Gatza ML, Blobe GC (2013). TbetaRIII/beta-arrestin2 regulates integrin alpha5beta1 trafficking, function, and localization in epithelial cells. Oncogene 32, 1416–1427.
Panetti TS, McKeown-Longo PJ (1993). The alpha v beta 5 integrin receptor regulates receptor-mediated endocytosis of vitronectin. J Biol Chem 268, 11492–11495.
Pankov R, Cukierman E, Katz BZ, Matsumoto K, Lin DC, Lin S, Hahn C, Yamada KM (2000). Integrin dynamics and matrix assembly: tensin-dependent translocation of alpha(5)beta(1) integrins promotes early fibronectin fibrillogenesis. J Cell Biol 148, 1075–1090.
Park J, Schwarzbauer JE (2014). Mammary epithelial cell interactions with fibronectin stimulate epithelial-mesenchymal transition. Oncogene 33, 1649–1657.
Pellinen T, Ivaska J (2006). Integrin traffic. J Cell Sci 119, 3723–3731.
Penheiter SG, Mitchell H, Garamszegi N, Edens M, Dore JJ Jr, Leof EB (2002). Internalization-dependent and -independent requirements for transforming growth factor beta receptor signaling via the Smad pathway. Mol Cell Biol 22, 4750–4759.
Rechtman MM, Nakaryakov A, Shapira KE, Ehrlich M, Henis YI (2009). Different domains regulate homomeric and heteromeric complex formation among type I and type II transforming growth factor-beta receptors. J Biol Chem 284, 7843–7852.
Ren M, Xu G, Zeng J, De Lemos-Chiarandini C, Adesnik M, Sabatini DD (1998). Hydrolysis of GTP on rab11 is required for the direct delivery of transferrin from the pericentriolar recycling compartment to the cell surface but not from sorting endosomes. Proc Natl Acad Sci USA 95, 6187–6192.
Roberts CJ, Birkenmeier TM, McQuillan JJ, Akiyama SK, Yamada SS, Chen WT, Yamada KM, McDonald JA (1988). Transforming growth factor beta stimulates the expression of fibronectin and of both subunits of the human fibronectin receptor by cultured human lung fibroblasts. J Biol Chem 263, 4586–4592.
Roberts M, Barry S, Woods A, van der Sluijs P, Norman J (2001). PDGF-regulated rab4-dependent recycling of alphavbeta3 integrin from early endosomes is necessary for cell adhesion and spreading. Curr Biol 11, 1392–1402.
Ruoslahti E (1984). Fibronectin in cell adhesion and invasion. Cancer Metastasis Rev 3, 43–51.
Sakai T, Larsen M, Yamada KM (2003). Fibronectin requirement in branching morphogenesis. Nature 423, 876–881.
Saulnier R, Bhardwaj B, Klassen J, Leopold D, Rahimi N, Tremblay E, Mosher D, Elliott B (1996). Fibronectin fibrils and growth factors stimulate anchorage-independent growth of a murine mammary carcinoma. Exp Cell Res 222, 360–369.
Schwarzbauer JE, DeSimone DW (2011). Fibronectins, their fibrillogenesis, and in vivo functions. Cold Spring Harb Perspect Biol 3, a005041.
Schwarzbauer JE, Sechler JL (1999). Fibronectin fibrillogenesis: a paradigm for extracellular matrix assembly. Cur Opin Cell Biol 11, 622–627.
Sechler JL, Takada Y, Schwarzbauer JE (1996). Altered rate of fibronectin matrix assembly by deletion of the first type III repeats. J Cell Biol 134, 573–583.
Shi F, Long X, Hendershot A, Miano JM, Sottile J (2014). Fibronectin matrix polymerization regulates smooth muscle cell phenotype through a Rac1 dependent mechanism. PLoS One 9, e94988.
Shi F, Sottile J (2008). Caveolin-1-dependent beta1 integrin endocytosis is a critical regulator of fibronectin turnover. J Cell Sci 121, 2360–2371.
Siegel PM, Shu W, Cardiff RD, Muller WJ, Massague J (2003). Transforming growth factor beta signaling impairs Neu-induced mammary tumorigenesis while promoting pulmonary metastasis. Proc Natl Acad Sci USA 100, 8430–8435.
Singh P, Schwarzbauer JE (2014). Fibronectin matrix assembly is essential for cell condensation during chondrogenesis. J Cell Sci 127, 4420–4428.
Song BD, Yarar D, Schmid SL (2004). An assembly-incompetent mutant establishes a requirement for dynamin self-assembly in clathrin-mediated endocytosis in vivo. Mol Biol Cell 15, 2243–2252.
Sottile J, Chandler J (2005). Fibronectin matrix turnover occurs through a caveolin-1-dependent process. Mol Biol Cell 16, 757–768.
Tomasini-Johansson BR, Annis DS, Mosher DF (2006). The N-terminal 70-kDa fragment of fibronectin binds to cell surface fibronectin assembly sites in the absence of intact fibronectin. Matrix Biol 25, 282–293.
Unlu G, Levic DS, Melville DB, Knapik EW (2014). Trafficking mechanisms of extracellular matrix macromolecules: insights from vertebrate development and human diseases. Int J Biochem Cell Biol 47, 57–67.
Wang SE, Wu FY, Shin I, Qu S, Arteaga CL (2005). Transforming growth factor β (TGF-β)-Smad target gene protein tyrosine phosphatase receptor type kappa is required for TGF-β function. Mol Cell Biol 25, 4703–4715.
Weigert R, Donaldson JG (2005). Fluorescent microscopy-based assays to study the role of Rab22a in clathrin-independent endocytosis. Methods Enzymol 403, 243–253.
Wendt MK, Tian M, Schiemann WP (2012). Deconstructing the mechanisms and consequences of TGF-beta-induced EMT during cancer progression. Cell Tissue Res 347, 85–101.
Wennerberg K, Lohikangas L, Gullberg D, Pfaff M, Johansson S, Fassler R (1996). Beta 1 integrin-dependent and -independent polymerization of fibronectin. J Cell Biol 132, 227–238.
Wrana JL, Attisano L, Carcamo J, Zentella A, Doody J, Laiho M, Wang XF, Massague J (1992). TGF beta signals through a heteromeric protein kinase receptor complex. Cell 71, 1003–1014.
Wu C, Hughes PE, Ginsberg MH, McDonald JA (1996). Identification of a new biological function for the integrin alpha v beta 3: initiation of fibronectin matrix assembly. Cell Adhes Commun 4, 149–158.
Yang JT, Bader BL, Kreidberg JA, Ullman-Cullere M, Trevithick JE, Hynes RO (1999). Overlapping and independent functions of fibronectin receptor integrins in early mesodermal development. Dev Biol 215, 264–277.
Yang JT, Hynes RO (1996). Fibronectin receptor functions in embryonic cells deficient in alpha 5 beta 1 integrin can be replaced by alpha V integrins. Mol Biol Cell 7, 1737–1748.
Yao D, Ehrlich M, Henis YI, Leof EB (2002). Transforming growth factor-beta receptors interact with AP2 by direct binding to beta2 subunit. Mol Biol Cell 13, 4001–4012.